Digital Signal Processing 19 (2009) 596–611

Contents lists available at ScienceDirect

Digital Signal Processing

www.elsevier.com/locate/dsp

A computationally efficient algorithm for joint range–DOA–frequency estimation of near-field sources

Junli Liang *,[1], Xianju Zeng, Bangjie Ji, Junying Zhang, Feng Zhao

National Key Laboratory of Underwater Information Process and Control, China Shipbuilding Industry Corp., Xi'an, China

ARTICLE INFO

Article history:
Available online 3 July 2008

Keywords:
Array signal processing
Near-field
Second-order statistics (SOS)

ABSTRACT

Near-field source localization using passive sensor arrays plays an important role in array signal processing areas. Although many algorithms have been developed to deal with this issue, most of them suffer from either parameter match or heavy loss of the aperture or high computational complexity problems. To overcome these problems, a new algorithm is proposed in this paper to jointly estimate the ranges, directions-of-arrival (DOAs), and frequencies of multiple near-field narrow-band sources. Simulation results verify that the proposed algorithm can resolve these problems and give much better performance.

1. Introduction

Near-field source localization using passive sensor arrays is widely applied in speech enhancement using microphone arrays, underwater source localization, ultrasonic imaging, electronic surveillance and seismic exploration applications. The estimation of near-field (i.e. Fresnel zone) source parameters is more complicated than that of the far-field case since the wavefront of near-field sources must be characterized by both direction-of-arrival (DOA) and range parameters [1–14]. In this case, the range information must be incorporated into the signal model. Therefore, the classical DOA estimation methods for far-field sources are no longer applicable to near-field case.

Recently, many approaches have been developed to deal with the near-field source localization problem (i.e. joint range-DOA estimation problem), such as the Maximum Likelihood method [2], the two-dimensional MUSIC method [3–5], the weighted linear prediction method [8–10], and the higher-order ESPRIT methods [11–13]. However, most of these methods either suffer from the heavy computational load due to the spectral peak search [2,3,5], iteration process [2], and computation of cumulant [11,12], or contain an additional parameters pairing procedure [8–12], or suffer from heavy loss of array aperture [8–12] (i.e. far less than M sources can be localized by M sensors, and thus hardware costs could be aggrandized), or cannot estimate the source frequencies simultaneously [2,3,5–12].

Few of the existing works dealt with passive three-dimensional (3-D) source localization, i.e. to jointly estimate the range, DOA, and frequency of near-field narrow-band source. To simultaneously estimate the frequencies of near-field sources, Chen proposed a cumulant-based algorithm [14]. However, this method needs to compare two sets of eigenvectors respectively with arbitrary orders (see Paragraph II on page 389 of [14] for details), and thus requires pairing parameters. In addition, it has high computational load because of the computation of cumulant.

To alleviate the computational overhead, avoid pairing parameters, and alleviate the loss of the aperture, a new algorithm for joint range-DOA-frequency estimation of near-field narrow-band sources is proposed in this paper. Although it is designed for near field sources, this algorithm can estimate some parameters of far field sources, such as DOA and frequency.

* Corresponding author.
E-mail address: heery_2004@hotmail.com (J. Liang).
[1] Present address: School of Computer Science and Engineering, Xi'an University of Technology, China.

1051-2004/$ – see front matter
doi:10.1016/j.dsp.2008.06.006

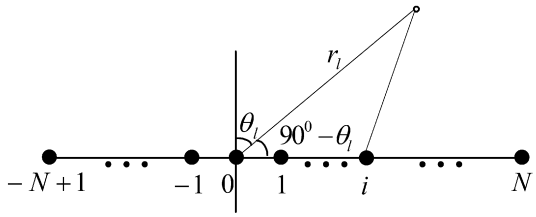

Fig. 1. Uniform linear array configuration.

Therefore, the proposed algorithm can deal with "any-field" sources, i.e. the total received signals by an array consists of either multiple near-field signals, or multiple far-field signals, or their mixture, which are often encountered in practical applications [14–18].

The rest of this paper is organized as follows. The signal model is introduced in Section 2. A 3-D near-field source localization algorithm is developed in Section 3. Simulation results are presented in Section 4. Conclusions are drawn in Section 5.

2. Problem formulation

Suppose that L near-field, narrow-band, independent radiating sources impinge on the uniform linear array (ULA) shown in Fig. 1. Let the 0th sensor be the phase reference point. Assume $s_l(t)e^{j2\pi f_l t}$ is the lth narrow-band source with center frequency f_l [17,18]. After being sampled with a proper rate f_s that satisfies the Nyquist rate, the signal received by the ith sensor can be expressed as [14]

$$x_i(k)=\sum_{l=1}^{L}s_l(k)e^{j\omega_l k}e^{j\tau_{il}}+n_i(k),\quad -N+1\leqslant i\leqslant N,\ k=0,\ldots,K-1, \tag{1}$$

where $s_l(k)e^{j\omega_l k}$ is the lth narrow-band signal with the normalized radian frequency $\omega_l=\frac{2\pi f_l}{f_s}$, K is the snapshot number, $\lambda_l=\frac{c}{f_l}=\frac{2\pi c}{\omega_l f_s}$ is the wavelength of the lth signal, and $n_i(k)$ is the additive white Gaussian noise (AWGN).

Let r_l be the distance between the lth source and the phase reference point. According to cosine theorem, the distance between the lth source and the ith sensor can be given by [10,11,14]

$$r_{il}=\sqrt{r_l^2+(id)^2-2r_l id\cos(90^\circ-\theta_l)}=r_l\sqrt{1+\frac{(id)^2}{r_l^2}-\frac{2id\sin\theta_l}{r_l}},\quad -N+1\leqslant i\leqslant N. \tag{2}$$

Therefore, the delay τ_{il}, which is associated with the lth source signal propagation time between the phase reference point and the ith sensor, can be given by in the three-dimensional localization case [10,11,14]:

$$\tau_{il}=\frac{2\pi(r_{i,l}-r_l)}{\lambda_l}=\frac{2\pi r_l}{\lambda_l}\left(\sqrt{1+\frac{(id)^2}{r_l^2}-\frac{2id\sin\theta_l}{r_l}}-1\right)\cong\gamma_l i+\phi_l i^2+O\left(\frac{d^2}{r_l^2}\right),\quad -N+1\leqslant i\leqslant N, \tag{3}$$

where τ_{il} is approximated by Fresnel approximation [10,11,14], which corresponds to the second-order Taylor expansion, $O(d^2/r_l^2)$ represents terms of order greater or equal to d^2/r_l^2 that neglected here. In addition, the parameters γ_l and ϕ_l are the functions of the azimuth θ_l and range r_l of the lth source [10,11,14]:

$$\gamma_l=-2\pi\frac{d}{\lambda_l}\sin(\theta_l) \tag{4}$$

and

$$\phi_l=\pi\frac{d^2}{\lambda_l r_l}\cos^2(\theta_l). \tag{5}$$

Using the above approximation in (3), the signal received by the ith sensor can be approximately expressed as [14]

$$x_i(k)=\sum_{l=1}^{L}s_l(k)e^{j\omega_l k}e^{j(i\gamma_l+i^2\phi_l)}+n_i(k),\quad -N+1\leqslant i\leqslant N. \tag{6}$$

In a matrix form, (6) can be written as

$$\mathbf{x}(k)=\mathbf{A}\mathbf{s}(k)+\mathbf{n}(k),\quad k=0,\ldots,K-1, \tag{7}$$

where

$$\mathbf{A} = [\,\mathbf{a}_1 \quad \dots \quad \mathbf{a}_L\,] = \begin{bmatrix} e^{j[(-N+1)\gamma_1+(-N+1)^2\phi_1]} & \dots & e^{j[(-N+1)\gamma_L+(-N+1)^2\phi_L]} \\ e^{j[(-N+2)\gamma_1+(-N+2)^2\phi_1]} & \dots & e^{j[(-N+2)\gamma_L+(-N+2)^2\phi_L]} \\ \vdots & \vdots & \vdots \\ 1 & \cdots & 1 \\ e^{j[\gamma_1+\phi_1]} & \dots & e^{j[\gamma_L+\phi_L]} \\ e^{j[2\gamma_1+4\phi_1]} & \dots & e^{j[2\gamma_L+4\phi_L]} \\ \vdots & \vdots & \vdots \\ e^{j[N\gamma_1+N^2\phi_1]} & \dots & e^{j[N\gamma_L+N^2\phi_L]} \end{bmatrix}, \tag{8}$$

$$\mathbf{n}(k) = \big[n_{-N+1}(k), n_{-N+2}(k), \dots, n_0(k), n_1(k), n_2(k), \dots, n_N(k)\big]^T, \tag{9}$$

$$\mathbf{s}(k) = \big[s_1(k)e^{j\omega_1 k}, \dots, s_L(k)e^{j\omega_L k}\big]^T, \tag{10}$$

and

$$\mathbf{x}(k) = \big[x_{-N+1}(k), x_{-N+2}(k), \dots, x_0(k), x_1(k), x_2(k), \dots, x_N(k)\big]^T. \tag{11}$$

Note that Fresnel zone (i.e. near-field) lies in the radiating zone $[\frac{1}{2\pi}\lambda_l, \frac{1}{\lambda_l}2D^2]$, where D is the array dimension (see [19] for details), and in this case ϕ_l cannot be neglected. However, in the far-field case, i.e. the radiating zone beyond $[0, \frac{1}{\lambda_l}2D^2]$, ϕ_l can be approximated by zero due to farther ranges of far-field sources (see Eq. (5)). Therefore, the far-field case can be looked upon as the special one of the near-field case, where $\phi_l = 0$. In fact the first-order Taylor expansion of (3) leads to the parametric model used in the far-field source localization problem.

For convenience, the common far-field signal model [17,18] is given by

$$x_i(k) = \sum_{l=1}^{L} s_l(k)e^{j\omega_l k}e^{j(i\gamma_l)} + n_i(k), \quad -N+1 \leqslant i \leqslant N,\ k = 0, \dots, K-1, \tag{12}$$

where $\phi_l = 0$.

The objective of this paper is to jointly estimate the 3-D parameters $\{r_l, \theta_l, \omega_l\}$ for near-field sources but the 2-D parameters $\{\theta_l, \omega_l\}$ for far-field sources, given the array data $\mathbf{x}(k)$ for $k = 0, \dots, K-1$.

Throughout the rest of the paper, the following hypotheses are assumed to hold:

(1) The source signals are statistically mutually independent, narrow-band stationary processes with nonzero power;
(2) The sensor noise is AWGN, and independent of the source signals;
(3) The matrix $\mathbf{A}$ has full rank L;
(4) The array is a ULA with element spacing $d \leqslant \min(\lambda_l/4)$;
(5) The source number $L < 2N$ is assumed in this paper, being different from those of [10,11,14] where $L < N$ is required.

3. Proposed algorithm

To develop a new joint estimation algorithm, we begin with the auto-correlation matrix of $\mathbf{x}(k)$, which can be expressed as

$$\mathbf{R}_1 = E\big[\mathbf{x}(k)\mathbf{x}^H(k)\big] = \mathbf{A}\mathbf{R}_s\mathbf{A}^H + \sigma_n^2\mathbf{I}_{2N} = \mathbf{R}_2 + \sigma_n^2\mathbf{I}_{2N}, \tag{13}$$

where

$$\mathbf{R}_2 = \mathbf{A}\mathbf{R}_s\mathbf{A}^H \tag{14}$$

and

$$\mathbf{R}_s = \operatorname{diag}[r_{s1}, r_{s2}, \dots, r_{sL}] = \operatorname{diag}\big[E\big(s_1(k)s_1^*(k)\big), E\big(s_2(k)s_2^*(k)\big), \dots, E\big(s_L(k)s_L^*(k)\big)\big]. \tag{15}$$

Let

$$\mathbf{\Phi}_1 = \operatorname{diag}[e^{j\omega_1}, e^{j\omega_2}, \dots, e^{j\omega_L}], \tag{16}$$

and we have

$$\mathbf{s}(k+1) \cong \mathbf{\Phi}_1\mathbf{s}(k), \tag{17}$$

under the narrow-band assumption as those of [17,18].

According to (17) and for different time lag, we define another second-order statistics (SOS) matrix

$$\mathbf{R}_3 = E\big[\mathbf{x}(k+1)\mathbf{x}^H(k)\big] \cong \mathbf{A}\mathbf{\Phi}_1\mathbf{R}_s\mathbf{A}^H. \tag{18}$$

Based on the hypotheses in Section 2, $\mathbf{R}_3$ is a $(2N \times 2N)$-dimensional matrix with full column rank L. In practice, $\mathbf{R}_1$ and $\mathbf{R}_3$ must be estimated from available K snapshots, i.e.

$$\hat{\mathbf{R}}_1 = \frac{1}{K}\sum_{k=0}^{K-1}\mathbf{x}(k)\mathbf{x}^H(k) \tag{19}$$

and

$$\hat{\mathbf{R}}_3 = \frac{1}{K-1}\sum_{k=0}^{K-2}\mathbf{x}(k+1)\mathbf{x}^H(k). \tag{20}$$

The eigenvalue decomposition (EVD) of $\hat{\mathbf{R}}_1$ yields

$$\hat{\mathbf{R}}_1 = \mathbf{U}\mathbf{V}\mathbf{U}^H = [\mathbf{u}_1, \mathbf{u}_2, \ldots, \mathbf{u}_{2N}]\,\mathrm{diag}[v_1, v_2, \ldots, v_{2N}][\mathbf{u}_1, \mathbf{u}_2, \ldots, \mathbf{u}_{2N}]^H, \tag{21}$$

where $\mathbf{V}$ is the diagonal matrix with the eigenvalue arranged as $v_1 \geqslant v_2 \geqslant \cdots \geqslant v_L > v_{L+1} \geqslant \cdots \geqslant v_{2N} > 0$, and $\mathbf{U}^H\mathbf{U} = \mathbf{I}_{2N}$. Let $\mathbf{U}_s = [\mathbf{u}_1, \mathbf{u}_2, \ldots, \mathbf{u}_L]$ be the eigenvectors corresponding to the L largest eigenvalues, and thus we have $\mathbf{U}_s^H\mathbf{U}_s = \mathbf{I}_L$. Since the signal subspace $\mathbf{U}_s$ coincides with the range space of $\mathbf{A}$, there must exist a unique invertible matrix, such that $\mathbf{A} = \mathbf{U}_s\mathbf{T}$.

In fact, since the snapshot size is finite, the noise power σ_n^2 must be estimated and can be determined by averaging the $(2N - L)$ smallest eigenvalues:

$$\hat{\sigma}_n^2 = \frac{1}{2N-L}\sum_{l=L+1}^{2N} v_l. \tag{22}$$

Additionally, the estimate of $\mathbf{R}_2$ is given by

$$\hat{\mathbf{R}}_2 = \sum_{l=1}^{L}\big(v_l - \hat{\sigma}_n^2\big)\mathbf{u}_l\mathbf{u}_l^H = \sum_{l=1}^{L}\hat{v}_l\mathbf{u}_l\mathbf{u}_l^H, \tag{23}$$

where $\hat{v}_l = v_l - \hat{\sigma}_n^2$.

By virtue of $\hat{\mathbf{R}}_2$, we define its pseudoinverse matrix $\hat{\mathbf{R}}_2^{\#}$ as follows:

$$\hat{\mathbf{R}}_2^{\#} = \sum_{l=1}^{L}\hat{v}_l^{-1}\mathbf{u}_l\mathbf{u}_l^H = \mathbf{U}_s\mathbf{V}_s^{-1}\mathbf{U}_s^H, \tag{24}$$

where $\mathbf{V}_s = \mathrm{diag}[\hat{v}_1, \hat{v}_2, \ldots, \hat{v}_L]$.

It is easily proven that $\hat{\mathbf{R}}_2^{\#}$ satisfies with following equation (see Appendix A for details):

$$\hat{\mathbf{R}}_3\hat{\mathbf{R}}_2^{\#}\mathbf{A} \cong \mathbf{A}\boldsymbol{\Phi}_1. \tag{25}$$

From (25), we can see that $e^{j\omega_l}$ and $\mathbf{a}_l$ are just the eigenvalue and corresponding eigenvector of $\hat{\mathbf{R}}_3\hat{\mathbf{R}}_2^{\#}$. Let the EVD of $\hat{\mathbf{R}}_3\hat{\mathbf{R}}_2^{\#}$ yield

$$\hat{\mathbf{R}}_3\hat{\mathbf{R}}_2^{\#} = \mathbf{B}_1\mathbf{C}_1\mathbf{B}_1^{-1} = [\mathbf{b}_1, \mathbf{b}_2, \ldots, \mathbf{b}_{2N}]\,\mathrm{diag}[c_1, c_2, \ldots, c_{2N}][\mathbf{b}_1, \mathbf{b}_2, \cdots, \mathbf{b}_{2N}]^{-1}, \tag{26}$$

where $|c_1| \geqslant |c_2| \geqslant \cdots \geqslant |c_L| > |c_{L+1}| \geqslant \cdots \geqslant |c_{2N}|$.

Based on Eqs. (8), (25), and (26), the estimates of ω_l and $\mathbf{a}_l$ can be given by

$$\hat{\omega}_l = \arg(c_l) \tag{27}$$

and

$$\hat{\mathbf{a}}_l = \frac{\mathbf{b}_l}{\mathbf{b}_l(N)}. \tag{28}$$

Based on $\hat{\mathbf{a}}_l$, we can form two $(2N - 1)$-dimensional column vectors as follows (see Appendix B for details):

$$\mathbf{d}_l = \begin{bmatrix} \hat{\mathbf{a}}_l(2)\hat{\mathbf{a}}_l^*(1)\hat{\mathbf{a}}_l^*(2)\hat{\mathbf{a}}_l(1) \\ \hat{\mathbf{a}}_l(3)\hat{\mathbf{a}}_l^*(2)\hat{\mathbf{a}}_l^*(2)\hat{\mathbf{a}}_l(1) \\ \vdots \\ \hat{\mathbf{a}}_l(2N-1)\hat{\mathbf{a}}_l^*(2N-2)\hat{\mathbf{a}}_l^*(2)\hat{\mathbf{a}}_l(1) \\ \hat{\mathbf{a}}_l(2N)\hat{\mathbf{a}}_l^*(2N-1)\hat{\mathbf{a}}_l^*(2)\hat{\mathbf{a}}_l(1) \end{bmatrix} = \begin{bmatrix} 1 \\ e^{j2\hat{\phi}_l} \\ \vdots \\ e^{j(4N-6)\hat{\phi}_l} \\ e^{j(4N-4)\hat{\phi}_l} \end{bmatrix} \tag{29}$$

and

$$\mathbf{e}_l = \begin{bmatrix} \hat{\mathbf{a}}_l(2)\hat{\mathbf{a}}_l^*(1)\hat{\mathbf{a}}_l^*(2N-2)\hat{\mathbf{a}}_l(2N-1) \\ \hat{\mathbf{a}}_l(3)\hat{\mathbf{a}}_l^*(2)\hat{\mathbf{a}}_l^*(2N-2)\hat{\mathbf{a}}_l(2N-1) \\ \vdots \\ \hat{\mathbf{a}}_l(2N-1)\hat{\mathbf{a}}_l^*(2N-2)\hat{\mathbf{a}}_l^*(2N-2)\hat{\mathbf{a}}_l(2N-1) \\ \hat{\mathbf{a}}_l(2N)\hat{\mathbf{a}}_l^*(2N-1)\hat{\mathbf{a}}_l^*(2N-2)\hat{\mathbf{a}}_l(2N-1) \end{bmatrix} = \begin{bmatrix} e^{j2\hat{\gamma}_l} \\ e^{j[2\hat{\phi}_l+2\hat{\gamma}_l]} \\ \vdots \\ e^{j[(4N-6)\hat{\phi}_l+2\hat{\gamma}_l]} \\ e^{j[(4N-4)\hat{\phi}_l+2\hat{\gamma}_l]} \end{bmatrix}, \tag{30}$$

where the superscript * denotes the complex conjugate. Based on $\mathbf{d}_l$ and $\mathbf{e}_l$, the estimates of $\{\gamma_l, \phi_l\}$ can be given by

$$\hat{\gamma}_l = \frac{1}{4N-2}\sum_{i=1}^{2N-1} \arg\left(\frac{\mathbf{e}_l(i)}{\mathbf{d}_l(i)}\right) \tag{31}$$

and

$$\hat{\phi}_l = \frac{1}{8N-8}\left[\sum_{i=1}^{2N-2} \arg\left(\frac{\mathbf{d}_l(i+1)}{\mathbf{d}_l(i)}\right) + \sum_{i=1}^{2N-2} \arg\left(\frac{\mathbf{e}_l(i+1)}{\mathbf{e}_l(i)}\right)\right]. \tag{32}$$

The wavelength estimate $\hat{\lambda}_l$ of the lth source is easily obtained from $\hat{\omega}_l$. According to (4), (5), (31), and (32), the azimuth and range estimates of the lth source can be in turn expressed as

$$\hat{\theta}_l = \arcsin\left(-\frac{\hat{\gamma}_l\hat{\lambda}_l}{2\pi d}\right) \tag{33}$$

and

$$\hat{r}_l = \frac{\pi d^2}{\hat{\lambda}_l\hat{\phi}_l}\cos^2(\hat{\theta}_l). \tag{34}$$

In fact, if the lth source is far-field one, the estimate $\hat{r}_l$ would be beyond $[0, \frac{1}{\lambda_l}2D^2]$ (see [19] for details). Thus, we can easily determine whether the lth source be near-field or far-field one.

Our algorithm constructs two $(2N \times 2N)$-dimensional SOS matrices using $2N$ sensors. Based on the subspace theory [4, 13], at least one dimension is left as the noise subspace, and thus our algorithm can at most deal with $(2N-1)$ sources. In addition, 3-D source parameters can be simultaneously estimated from the associated eigenvector and eigenvalue of $\hat{\mathbf{R}}_3\hat{\mathbf{R}}_2^{\#}$, so the proposed algorithm is one that avoids pairing parameters. Regarding the main computational complexity, we only consider the multiplications involved in calculating the matrices and in performing the EVD of matrix. The proposed algorithm requires $[2 \times ((2N)^2K)]$ to estimate two $(2N \times 2N)$-dimensional SOS matrices, and needs $[2 \times (\frac{4}{3}(2N)^3)]$ to decompose two $(2N \times 2N)$-dimensional SOS matrices. Here K and $2N$ stand for the snapshot and sensor number, respectively.

The algorithm in [14] constructs three $(N \times N)$-dimensional cumulant matrices (i.e. $\mathbf{C}_1$, $\mathbf{C}_2$, and $\mathbf{C}_3$, see Eqs. (10), (15), and (16) of [14] for details) using $2N$ sensors, and thus can localize at most $(N-1)$ sources. The algorithm in [14] forms two new matrices, i.e. $\mathbf{C}_2^H\mathbf{C}_1^{\#}$ and $\mathbf{C}_3^H\mathbf{C}_1^{\#}$ (see Eqs. (19) and (20) of [14] for details), which have the similar forms as $\hat{\mathbf{R}}_3\hat{\mathbf{R}}_2^{\#}$ mentioned above. Finally, it uses the eigenvectors and eigenvalues, which are yielded from the EVDs of $\mathbf{C}_2^H\mathbf{C}_1^{\#}$ and $\mathbf{C}_3^H\mathbf{C}_1^{\#}$, to jointly estimate the range–DOA–frequency of near-field narrow-band sources. Although $\mathbf{C}_2^H\mathbf{C}_1^{\#}$ and $\mathbf{C}_3^H\mathbf{C}_1^{\#}$ have the same L eigenvectors corresponding to their respective L nonzero eigenvalues, their EVDs yield two set of eigenvectors with arbitrary orders. Therefore, the algorithm in [14] needs to match them by contrasting the two set of eigenvectors (see Paragraph II on page 389 of [14] for details). It is obvious that the algorithm in [14] requires pairing parameters. Besides, the method in [14] requires $(3 \times (9N^2K))$ to compute three $(N \times N)$-dimensional cumulant matrices, and needs $(2 \times (\frac{4}{3}N^3))$ to decompose two $(N \times N)$-dimensional cumulant matrices.

In general case,$K \gg 2N$, so the proposed algorithm is more computationally efficient than that of [14]. Besides, we can see that our algorithm, which avoids pairing parameters, makes more efficient use of the array aperture, so it has higher estimate accuracy than that of [14].

4. Simulation results

Some simulations are conducted in this section to assess the proposed algorithm. We consider a 6-element ULA with element spacing $d = \min(\lambda_l/4)$. The sampling rate is 20 MHz. Two equal-power, statistically independent narrow-band sources (bandwidth = 25 kHz), respectively with center frequency 2.0 and 3.0 MHz (i.e. $\omega_1 = \frac{2\pi \times 2.0\ \mathrm{M}}{20\ \mathrm{M}} = 0.2\pi$ rad/s, $\lambda_1 = \frac{3\times 10^8}{2.0\times 10^6} = 150$, $\omega_2 = \frac{2\pi \times 3.0\ \mathrm{M}}{20\ \mathrm{M}} = 0.3\pi$ rad/s, and $\lambda_2 = \frac{3\times 10^8}{3.0\times 10^6} = 100$), radiate on the array. And the received signals are polluted by zero-mean AWGN. For comparison, we simultaneously execute the algorithm in [14], called "Chen" in the following experiments and figures. At the same time the related Cramer–Rao lower bounds (CRLB) for estimating source parameters are obtained from the inverse of Fisher information matrix [20] (see Appendix C for details), and shown in the

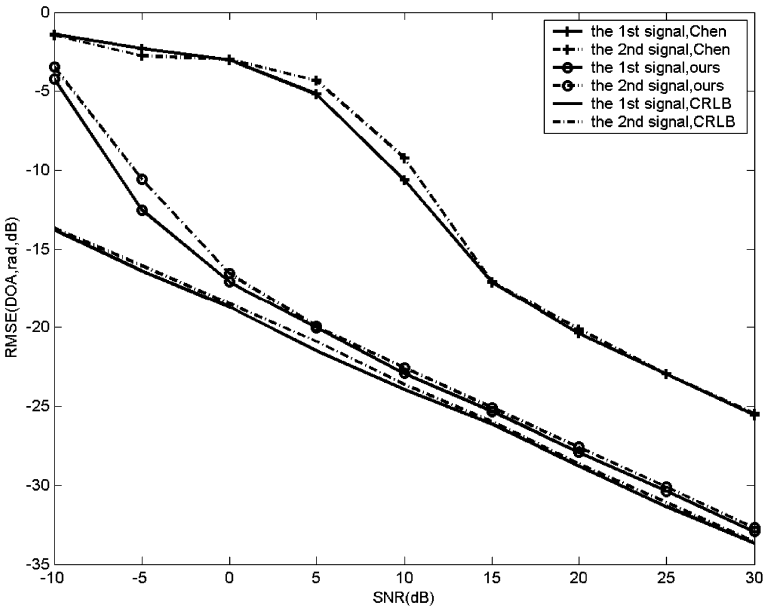

Fig. 2. RMSE of the DOAs versus SNR (two near-field sources).

relevant figures. The DOA, frequency, and range estimates are scaled in units of rad, rad/s, and wavelength, respectively. And the performance of these algorithms is measured by the estimated root mean-square error (RMSE) of 500 independent Monte Carlo runs. To explain the RMSE definition of these estimates, we take the range RMSE of the lth near-field source for example:

$$\mathrm{RMSE} = 10 \times \log_{10} \sqrt{\frac{1}{500} \sum_{i=1}^{500} \left(\frac{\hat{r}_{il}}{\hat{\lambda}_l} - \frac{r_l}{\lambda_l} \right)^2}, \tag{35}$$

where r_l is the true value. The RMSEs of other parameters, such as DOA and frequency estimates of near-field or far-field sources, have the similar form as that of (35).

In fact, we would obtain the "range estimates" of far-field sources from the above-mentioned algorithm. In this case, we can determine whether it is a far-field or near-field source by comparing the "range estimate" with the threshold value $2D^2/\hat{\lambda}_l$ (see [19] for details). Therefore, the "range estimate" of far-field sources cannot be given in the following experiment results because it is generally farther larger than the threshold value $2D^2/\hat{\lambda}_l$.

In the first experiment, the proposed algorithm is used to deal with the pure near-filed case, and the effect of signal-to-noise (SNR) on the performance of the proposed algorithm is investigated. The two near-field sources are located at $\{\theta_1 = 10^\circ,\ r_1 = 0.5\lambda_1\}$ and $\{\theta_2 = 20^\circ,\ r_2 = 1.0\lambda_2\}$, respectively. The snapshot number is set equal to 400, and the SNR varies from -10 to 30 dB. Figs. 2, 3, and 4 show the RMSE of the DOA, frequency, and range estimates of the two sources, respectively.

In the second experiment, the proposed algorithm is still used to deal with the pure near-filed case, and the influence of snapshot number on the performance of the proposed algorithm is investigated. The two near-field sources are located at $\{\theta_1 = 10^\circ,\ r_1 = 0.5\lambda_1\}$ and $\{\theta_2 = 20^\circ,\ r_2 = 1.0\lambda_2\}$, respectively. The SNR is set equal to 10 dB, and the snapshot number varies from 50 to 2000. Figs. 5, 6, and 7 show the RMSE of the DOA, frequency, and range estimates of the two sources, respectively.

From the first and second experiments, we can see that our algorithm has higher estimation accuracy than that of [14]. In addition, the RMSE of the range estimate of the first source (closer to the array) is much lower than that of the second source.

Note that the virtual "steering matrix" $\mathbf{A}_1$ defined in Eqs. (10) and (11) of [14] has the following form:

$$\mathbf{A}_1 = \begin{bmatrix} 1 & 1 & \cdots & 1 \\ e^{j2\phi_1} & e^{j2\phi_2} & \cdots & e^{j2\phi_L} \\ \vdots & \vdots & \cdots & \vdots \\ e^{j2(N-1)\phi_1} & e^{j2(N-1)\phi_2} & \cdots & e^{j2(N-1)\phi_L} \end{bmatrix}. \tag{36}$$

If the lth source is far-field one, $\phi_l = 0$ and the lth column of this virtual "steering matrix" becomes unit column vector, i.e. $[\underbrace{1 \ \ldots \ 1}_{N}]^T$.

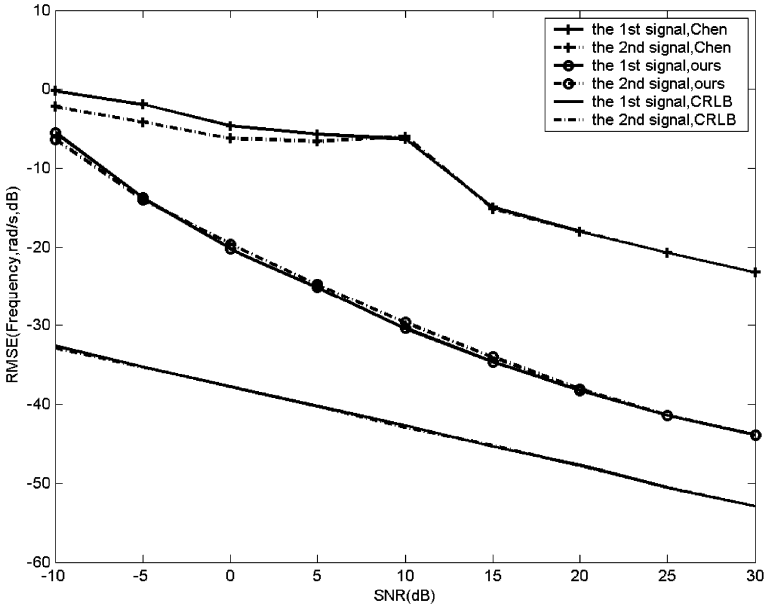

Fig. 3. RMSE of the frequencies versus SNR (two near-field sources).

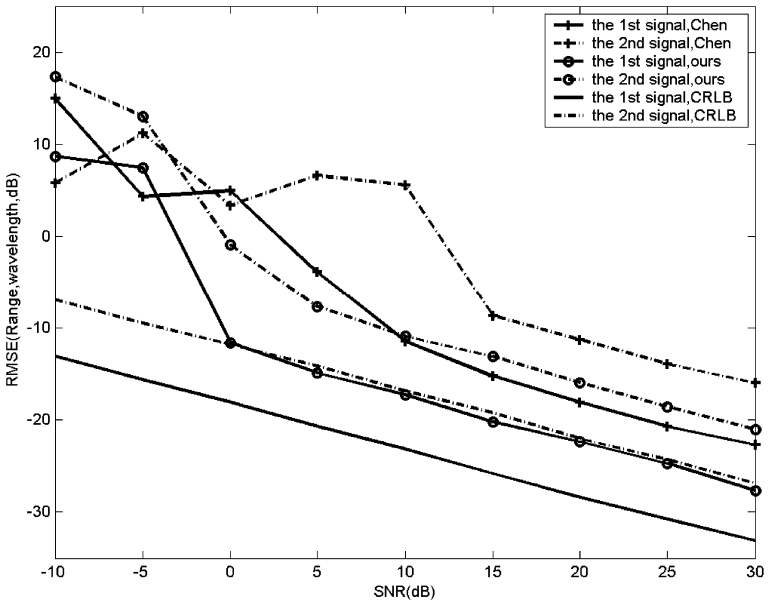

Fig. 4. RMSE of the ranges versus SNR (two near-field sources).

To assess the ability of the proposed algorithm to deal with mixed far-field and near-field sources, we take the following two cases into accounts:

(1) One far-field source and one near-field source are considered in the third and fourth experiments.

In the third experiment, the proposed algorithm is used to deal with one near-filed source and one far-field source, and the effect of SNR on the performance of the proposed algorithm is investigated. The near-field source is located at $\{\theta_1 = 10^\circ, r_1 = 0.5\lambda_1\}$, while the far-field one is located at $\{\theta_2 = 20^\circ\}$. The snapshot number is set equal to 400, and the SNR varies from -10 to 30 dB. Figs. 8, 9, and 10 show the RMSE of the DOA, frequency, and range (only near-field source is considered) estimates of the two sources, respectively.

In the fourth experiment, the proposed algorithm is still used to deal with one near-filed source and one far-field source, and the influence of snapshot number on the performance of the proposed algorithm is investigated. The near-field source is located at $\{\theta_1 = 10^\circ, r_1 = 0.5\lambda_1\}$, while the far-field one is located at $\{\theta_2 = 20^\circ\}$. The SNR is set equal to 10 dB, and

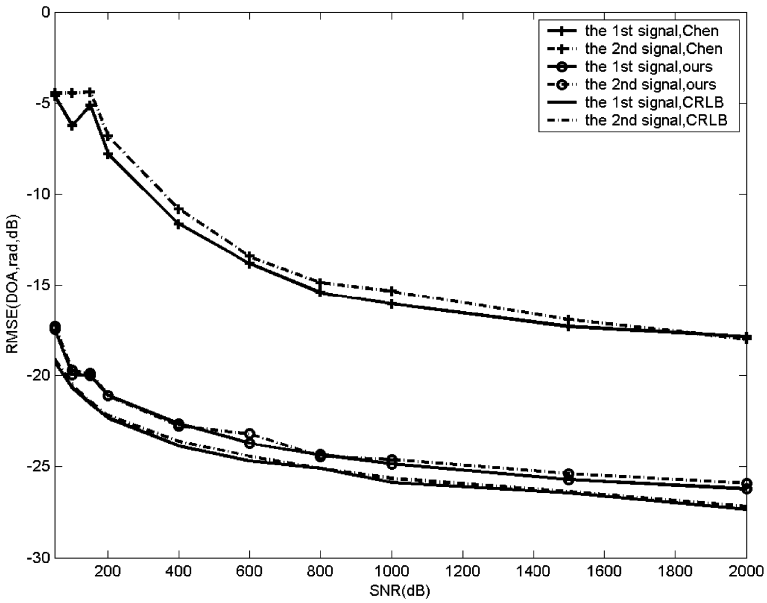

Fig. 5. RMSE of the DOAs versus snapshot number (two near-field sources).

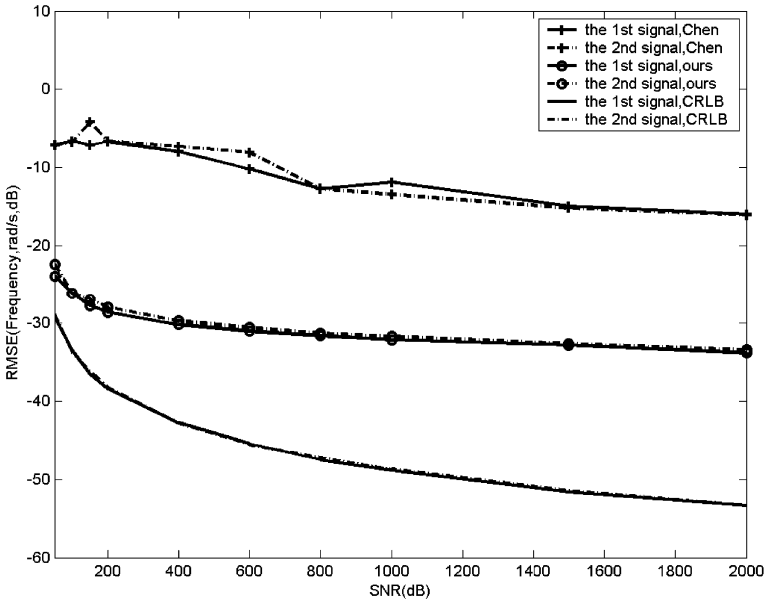

Fig. 6. RMSE of the frequencies versus snapshot number (two near-field sources).

the snapshot number varies from 50 to 2000. Figs. 11, 12, and 13 show the RMSE of the DOA, frequency, and range (only near-field source is considered) estimates of the two sources, respectively.

From the third and fourth experiments, we can see that our algorithm still has higher estimation accuracy than that of [14]. The two algorithms can be applied to mixed near-field and far-field sources, where only one far-field source exists. In this case, the virtual "steering matrix" $\mathbf{A}_1$ still has full rank. Therefore, the algorithm in [14] can also be deal with this case.

(2) However, when more than one far-field sources exist, the virtual "steering matrix" $\mathbf{A}_1$ in [14] has at least two unit column vectors (see Eq. (36)), and thus no longer has full rank. Therefore, the algorithm in [14] becomes invalid. To assess the ability of our algorithm to deal with this case, we introduce the following two experiments.

In the fifth experiment, the proposed algorithm is used to deal with the pure far-field case, and the effect of SNR on the performance of the proposed algorithm is investigated. The two far-field sources are located at $\{\theta_1 = 10^\circ\}$ and $\{\theta_2 = 20^\circ\}$, respectively. The snapshot number is set equal to 400, and the SNR varies from -10 to 30 dB. Figs. 14 and 15 show the RMSE of the DOA and frequency estimates of the two far-field sources, respectively.

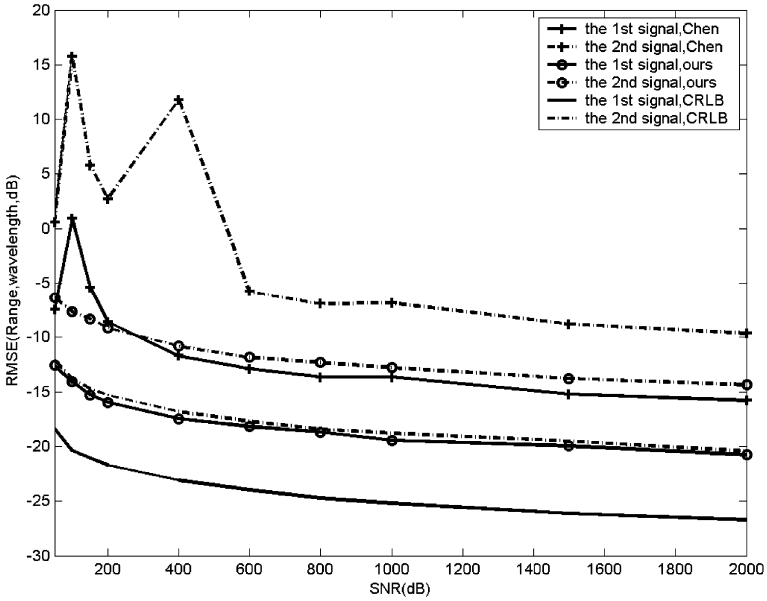

Fig. 7. RMSE of the ranges versus snapshot number (two near-field sources).

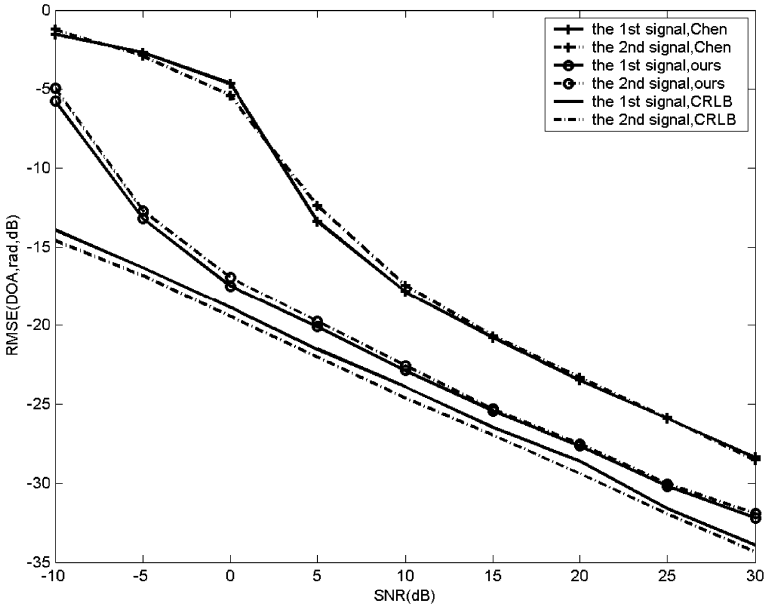

Fig. 8. RMSE of the DOAs versus SNR (one near-field source and one far-field source).

In the sixth experiment, the proposed algorithm is still used to deal with the pure far-field case, and the influence of snapshot number on the performance of the proposed algorithm is investigated. The two far-field sources are located at $\{\theta_1 = 10^\circ\}$ and $\{\theta_2 = 20^\circ\}$, respectively. The SNR is set equal to 10 dB, and the snapshot number varies from 50 to 2000. Figs. 16 and 17 show the RMSE of the DOA and frequency estimates of the two far-field sources, respectively.

From the fifth and sixth experiments, we can see that our algorithm still has high estimation accuracy in this case. However, when more than one far-field sources exist, the matrix $\mathbf{A}_1$ defined in Eqs. (10) and (11) of [14] no longer has full rank (because at least two columns in $\mathbf{A}_1$ are unit column vectors, and $\mathbf{A}_1$ no longer has full column rank). Therefore, the algorithm in [14] becomes invalid in this case.

From all experiments, we can see that our algorithm has higher estimation accuracy than that of [14]. The success of our algorithm lies in the following: under the same sensor number, our algorithm constructs higher-dimension matrices ($(2N \times 2N)$-dimensional) than those of [14] ($(N \times N)$-dimensional). It is obvious that the algorithm in [14] suffers heavy aperture loss, which denotes that in some way our algorithm used more sensors than that of [14].

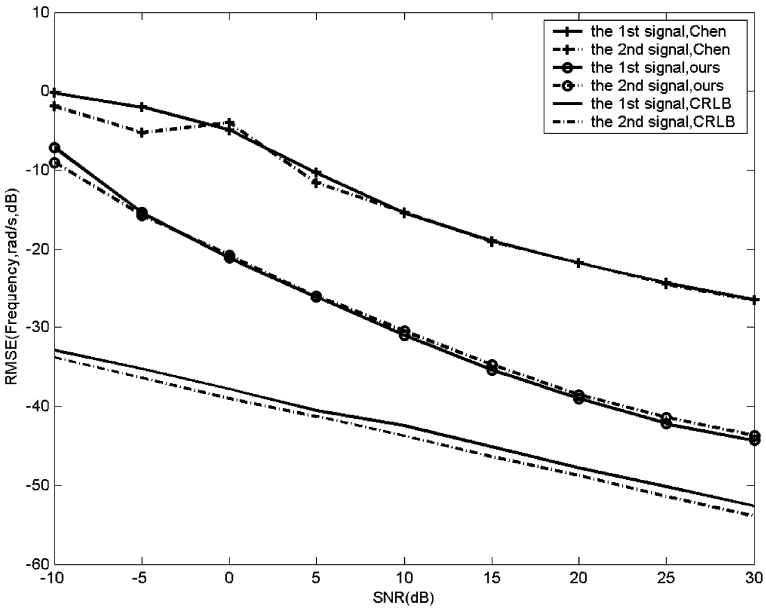

Fig. 9. RMSE of the frequencies versus SNR (one near-field source and one far-field source).

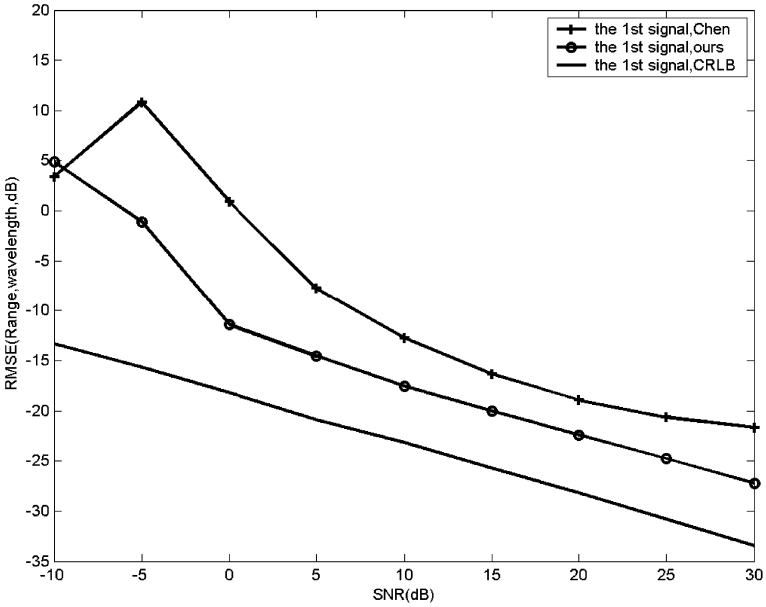

Fig. 10. RMSE of the range of the first source (only near-field source) versus SNR.

In addition, when more than one far-field sources exist, the virtual "steering matrix" $\mathbf{A}_1$ defined in Eqs. (10) and (11) of [14] no longer has full column rank. Therefore, the algorithm in [14] become invalid in this case. However, our algorithm can still ensure that the related steering matrix $\mathbf{A}$ has full rank (see Eq. (8)), so it is still applicable.

5. Conclusion

Based a uniform linear array, a computationally efficient algorithm based on SOS is presented for joint range–DOA–frequency estimation of multiple near-field narrow-band sources. The 3-D source parameters can be simultaneously estimated from the eigenvectors and corresponding eigenvalues of one matrix, and thus the proposed algorithm can avoid pairing parameters. In addition, the proposed algorithm makes efficient use of the array aperture, and has high estimation accuracy. What is more important, the proposed algorithm can be applied to deal with mixed near-field and far-filed sources.

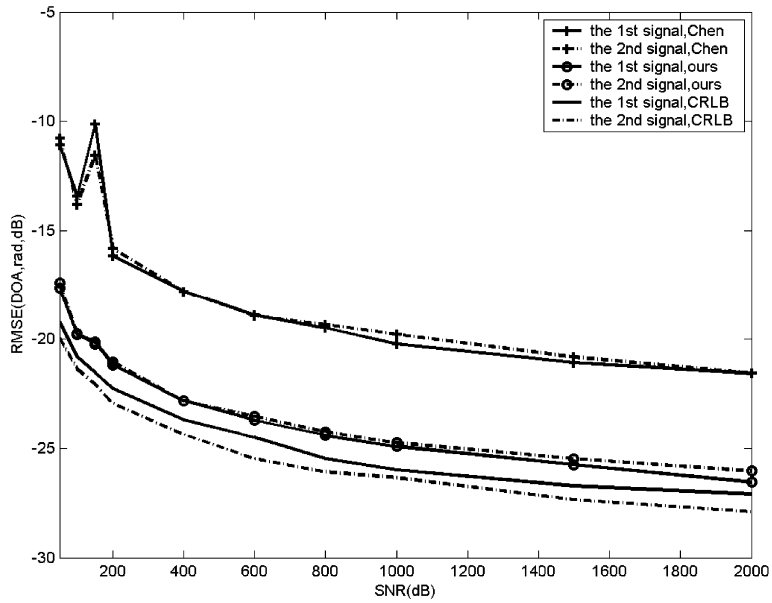

Fig. 11. RMSE of the DOAs versus snapshot number (one near-field source and one far-field source).

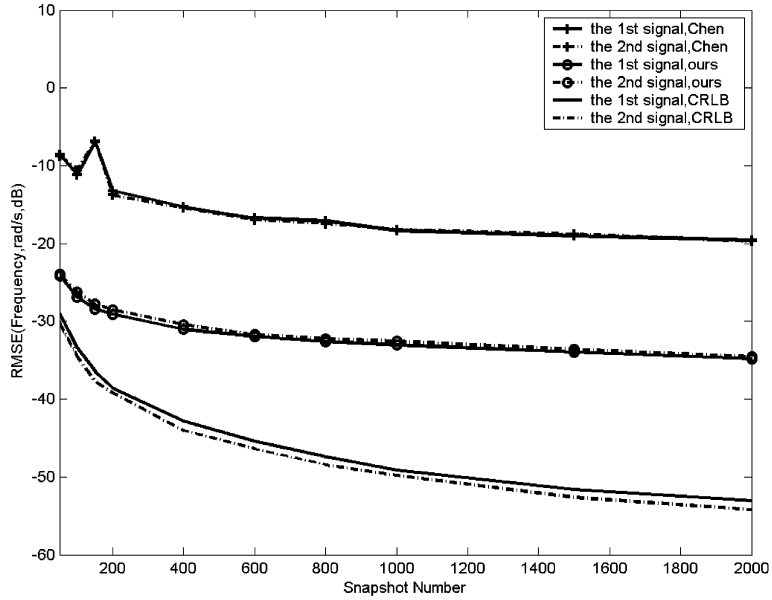

Fig. 12. RMSE of the frequencies versus snapshot number (one near-field source and one far-field source).

Acknowledgments

The authors would like to thank the editors and anonymous reviewers for their valuable comments and suggestions on this manuscript.

Appendix A

In this appendix, we prove (25). Note that the signal subspace $\mathbf{U}_s$ coincides with the range space of $\mathbf{A}$, and thus there must exist a unique invertible matrix, such that $\mathbf{A} = \mathbf{U}_s\mathbf{T}$. By using $\mathbf{A} = \mathbf{U}_s\mathbf{T}$, we in turn obtain

$$\begin{aligned}\mathbf{U}_s\mathbf{U}_s^H\mathbf{A} &= \mathbf{U}_s\mathbf{U}_s^H\left(\mathbf{U}_s\mathbf{T}\right)\\ &= \mathbf{U}_s\left(\mathbf{U}_s^H\mathbf{U}_s\right)\mathbf{T}\end{aligned}$$

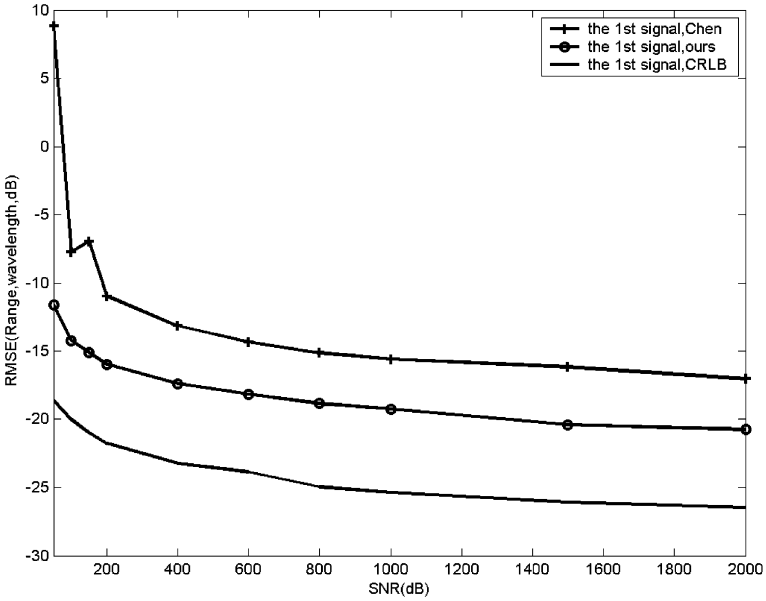

Fig. 13. RMSE of the range of the first source (only near-field source) versus snapshot number.

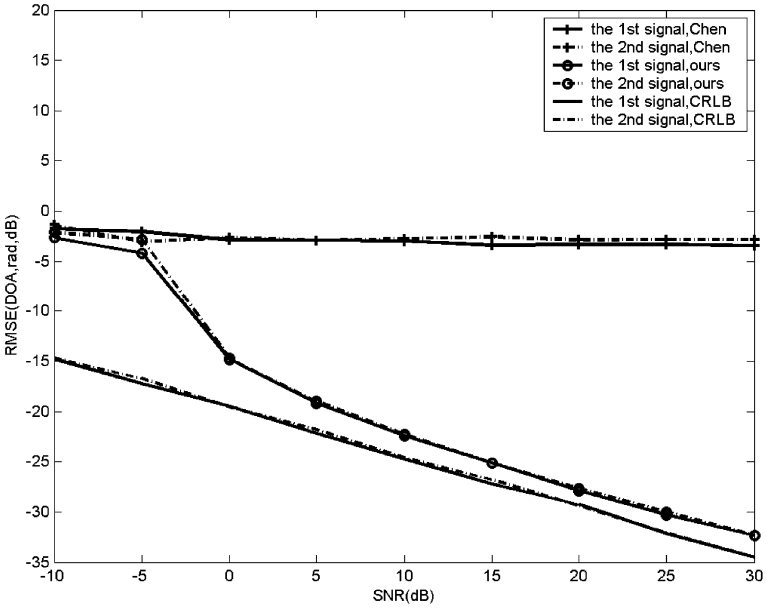

Fig. 14. RMSE of the DOAs versus SNR (two far-field sources).

$$= \mathbf{U}_S\mathbf{T}$$
$$= \mathbf{A} \tag{37}$$

and

$$\begin{aligned}\hat{\mathbf{R}}_3\hat{\mathbf{R}}_2^{\#}\mathbf{A} &\cong \mathbf{A}\boldsymbol{\Phi}_1\mathbf{R}_S\mathbf{A}^H\mathbf{U}_S\mathbf{V}_S^{-1}\mathbf{U}_S^H\mathbf{A}\\ &= \mathbf{A}\boldsymbol{\Phi}_1(\mathbf{A}^H\mathbf{A})^{-1}(\mathbf{A}^H\mathbf{A})\mathbf{R}_S\mathbf{A}^H\mathbf{U}_S\mathbf{V}_S^{-1}\mathbf{U}_S^H\mathbf{A}\\ &= \mathbf{A}\boldsymbol{\Phi}_1(\mathbf{A}^H\mathbf{A})^{-1}\mathbf{A}^H(\mathbf{A}\mathbf{R}_S\mathbf{A}^H)\mathbf{U}_S\mathbf{V}_S^{-1}\mathbf{U}_S^H\mathbf{A}\\ &= \mathbf{A}\boldsymbol{\Phi}_1(\mathbf{A}^H\mathbf{A})^{-1}\mathbf{A}^H\mathbf{R}_2\mathbf{U}_S\mathbf{V}_S^{-1}\mathbf{U}_S^H\mathbf{A}\\ &= \mathbf{A}\boldsymbol{\Phi}_1\left(\mathbf{A}^H\mathbf{A}\right)^{-1}\mathbf{A}^H\left(\mathbf{U}_S\mathbf{V}_S\mathbf{U}_S^H\right)\mathbf{U}_S\mathbf{V}_S^{-1}\mathbf{U}_S^H\mathbf{A}\end{aligned}$$

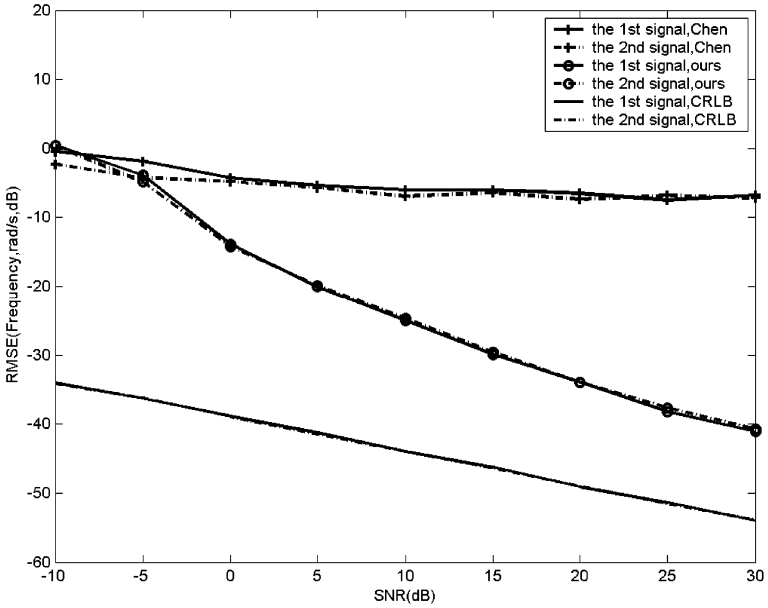

Fig. 15. RMSE of the frequencies versus SNR (two far-field sources).

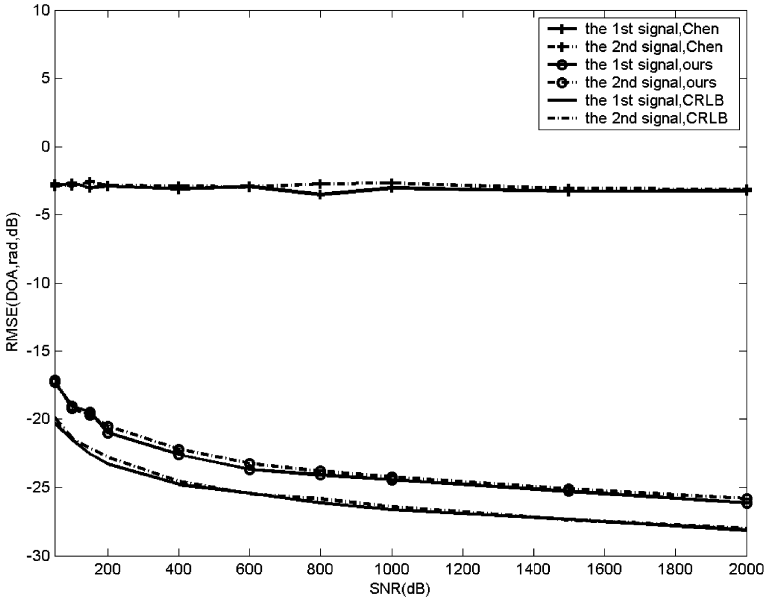

Fig. 16. RMSE of the DOAs versus snapshot number (two far-field sources).

$$
\begin{aligned}
&= \mathbf{A}\boldsymbol{\Phi}_1(\mathbf{A}^H\mathbf{A})^{-1}\mathbf{A}^H\mathbf{U}_s\mathbf{U}_s^H\mathbf{A} \\
&= \mathbf{A}\boldsymbol{\Phi}_1\big(\mathbf{A}^H\mathbf{A}\big)^{-1}\mathbf{A}^H\big(\mathbf{U}_s\mathbf{U}_s^H\mathbf{A}\big) \\
&= \mathbf{A}\boldsymbol{\Phi}_1(\mathbf{A}^H\mathbf{A})^{-1}\mathbf{A}^H\mathbf{A} \\
&= \mathbf{A}\boldsymbol{\Phi}_1. \qquad (38)
\end{aligned}
$$

Appendix B

In this appendix, we prove (29) and (30). From (8), we can see that the i element of $\hat{\mathbf{a}}_l$ has the following form:

$$\hat{\mathbf{a}}_l(i) = e^{j[(-N+i)\hat{\gamma}_l + (-N+i)^2\hat{\phi}_l]}. \qquad (39)$$

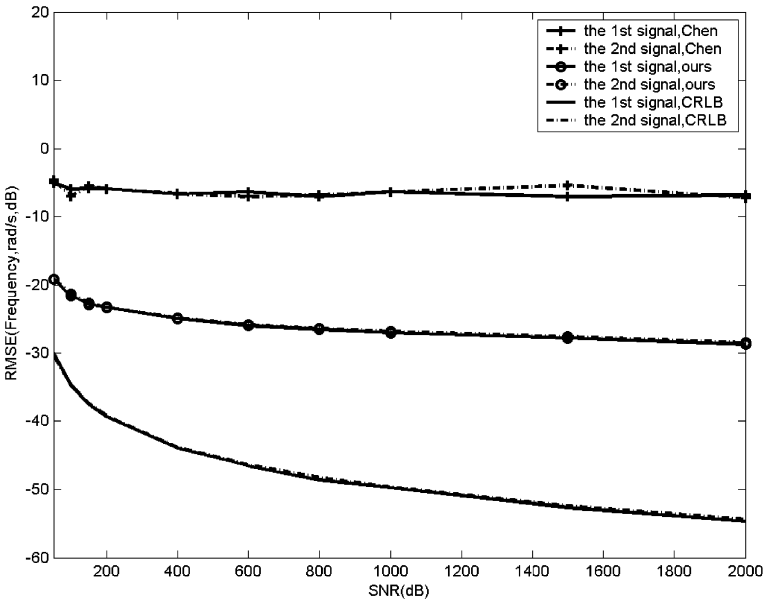

Fig. 17. RMSE of the frequencies versus snapshot number (two far-field sources).

By using (29), we have

$$\begin{aligned}\mathbf{d}_l(i) &= \hat{\mathbf{a}}_l(i+1)\hat{\mathbf{a}}_l^*(i)\hat{\mathbf{a}}_l^*(2)\hat{\mathbf{a}}_l(1)\\ &= e^{j[(-N+i+1)\hat{\gamma}_l+(-N+i+1)^2\hat{\phi}_l]}e^{-j[(-N+i)\hat{\gamma}_l+(-N+i)^2\hat{\phi}_l]}e^{-j[(-N+2)\hat{\gamma}_l+(-N+2)^2\hat{\phi}_l]}e^{j[(-N+1)\hat{\gamma}_l+(-N+1)^2\hat{\phi}_l]}\\ &= e^{j[(-N+i+1)-(-N+i)-(-N+2)+(-N+1)]\hat{\gamma}_l}e^{j[(-N+i+1)^2-(-N+i)^2-(-N+2)^2+(-N+1)^2]\hat{\phi}_l}\\ &= e^{j[2(i-1)\hat{\phi}_l]}\end{aligned} \tag{40}$$

and

$$\begin{aligned}\mathbf{e}_l(i) &= \hat{\mathbf{a}}_l(i+1)\hat{\mathbf{a}}_l^*(i)\hat{\mathbf{a}}_l^*(2N-2)\hat{\mathbf{a}}_l(2N-1)\\ &= e^{j[(-N+i+1)\hat{\gamma}_l+(-N+i+1)^2\hat{\phi}_l]}e^{-j[(-N+i)\hat{\gamma}_l+(-N+i)^2\hat{\phi}_l]}e^{-j[(N-2)\hat{\gamma}_l+(N-2)^2\hat{\phi}_l]}e^{j[(N-1)\hat{\gamma}_l+(N-1)^2\hat{\phi}_l]}\\ &= e^{j[(-N+i+1)-(-N+i)-(N-2)+(N-1)]\hat{\gamma}_l}e^{j[(-N+i+1)^2-(-N+i)^2-(N-2)^2+(N-1)^2]\hat{\phi}_l}\\ &= e^{j[2(i-1)\hat{\phi}_l+2\hat{\gamma}_l]}.\end{aligned} \tag{41}$$

Appendix C

In this appendix, we derive the CRLB for the estimated parameters. Note that the range estimates are scaled in unit of wavelength in Section 4, and we define the coefficient η_l as follows:

$$\eta_l = \frac{r_l}{\lambda_l}. \tag{42}$$

Therefore, ϕ_l in (5) can also be rewritten as

$$\phi_l = \pi\frac{d^2}{\lambda_l^2\eta_l}\cos^2(\theta_l). \tag{43}$$

In addition, by virtue of (6), we can obtain

$$n_i(k) = x_i(k) - \sum_{l=1}^{L} s_l(k)e^{j\omega_l k}e^{j(i\gamma_l+i^2\phi_l)}. \tag{44}$$

From (44), we define the probability density function $p(\mathbf{x}|\psi)$ as

$$p(\mathbf{x}|\psi) = \prod_{k=0}^{K-1}\prod_{i=-N+1}^{N}\frac{1}{\sqrt{2\pi\sigma^2}}e^{-\frac{1}{2\sigma^2}\left(x_i(k)-\sum_{l=1}^{L}s_l(k)e^{j\omega_l k}e^{j(i\gamma_l+i^2\phi_l)}\right)^H\left(x_i(k)-\sum_{l=1}^{L}s_l(k)e^{j\omega_l k}e^{j(i\gamma_l+i^2\phi_l)}\right)}, \tag{45}$$

where $\mathbf{x} = [\mathbf{x}(0), \mathbf{x}(1), \ldots, \mathbf{x}(K-1)]^T$ and $\psi = [\psi_1 \ \ldots \ \psi_l \ \ldots \ \psi_L]^T$. If the lth source is near-filed one, ψ_l is given by

$$\psi_l = [\,\omega_l \quad \theta_l \quad \eta_l\,]^T; \tag{46}$$

or else, for far-field source, it is expressed as

$$\psi_l = [\,\omega_l \quad \theta_l\,]^T. \tag{47}$$

The natural logarithm of $p(\mathbf{x}|\psi)$ can be expressed as

$$\ln\big(p(\mathbf{x}|\psi)\big) = -NK\ln(2\pi\sigma^2) - \frac{1}{2\sigma^2}\sum_{k=0}^{K-1}\sum_{i=-N+1}^{N}\left(x_i(k) - \sum_{l=1}^{L} s_l(k)e^{j\omega_l k}e^{j(i\gamma_l + i^2\phi_l)}\right)^H\left(x_i(k) - \sum_{l=1}^{L} s_l(k)e^{j\omega_l k}e^{j(i\gamma_l + i^2\phi_l)}\right). \tag{48}$$

Based on (45), (46), and (48), the partial derivative with respect to the three elements of ψ_l for the near-field case can be respectively given by

$$\frac{\partial \ln(p(\mathbf{x}|\psi))}{\partial \omega_l} = \frac{1}{\sigma^2}\sum_{k=0}^{K-1}\sum_{i=-N+1}^{N}\big\{\mathrm{Re}\big(jks_l(k)e^{j\omega_l k}e^{j(i\gamma_l + i^2\phi_l)}n_i^*(k)\big)\big\}, \tag{49}$$

$$\frac{\partial \ln(p(\mathbf{x}|\psi))}{\partial \theta_l} = \frac{1}{\sigma^2}\sum_{k=0}^{K-1}\sum_{i=-N+1}^{N}\left\{\mathrm{Re}\left[js_l(k)e^{j\omega_l k}e^{j(i\gamma_l + i^2\phi_l)}\left(-\frac{2\pi di\sin\theta_l}{\lambda_l} - \frac{\pi d^2 i^2\sin(2\theta_l)}{\lambda_l^2\eta_l}\right)n_i^*(k)\right]\right\}, \tag{50}$$

and

$$\frac{\partial \ln(p(\mathbf{x}|\psi))}{\partial \eta_l} = \frac{1}{\sigma^2}\sum_{k=0}^{K-1}\sum_{i=-N+1}^{N}\left\{\mathrm{Re}\left[js_l(k)e^{j\omega_l k}e^{j(i\gamma_l + i^2\phi_l)}\left(-\frac{\pi d^2 i^2\cos^2\theta_l}{\lambda_l^2\eta_l^2}\right)n_i^*(k)\right]\right\}. \tag{51}$$

Therefore, the partial derivative with respect to ψ_l for the near-field case can be expressed as

$$\frac{\partial \ln(p(\mathbf{x}|\psi))}{\partial \psi_l} = \left[\frac{\partial \ln(p(\mathbf{x}|\psi))}{\partial \omega_l} \quad \frac{\partial \ln(p(\mathbf{x}|\psi))}{\partial \theta_l} \quad \frac{\partial \ln(p(\mathbf{x}|\psi))}{\partial \eta_l}\right]^T. \tag{52}$$

If the lth source is far-filed one (see Eq. (12)), the partial derivative with respect to ψ_l can be expressed as

$$\frac{\partial \ln(p(\mathbf{x}|\psi))}{\partial \psi_l} = \left[\frac{\partial \ln(p(\mathbf{x}|\psi))}{\partial \omega_l} \quad \frac{\partial \ln(p(\mathbf{x}|\psi))}{\partial \theta_l}\right]^T, \tag{53}$$

where $\frac{\partial \ln(p(\mathbf{x}|\psi))}{\partial \omega_l}$ and $\frac{\partial \ln(p(\mathbf{x}|\psi))}{\partial \theta_l}$ are different from those of the near-field case and are respectively given by

$$\frac{\partial \ln(p(\mathbf{x}|\psi))}{\partial \omega_l} = \frac{1}{\sigma^2}\sum_{k=0}^{K-1}\sum_{i=-N+1}^{N}\big\{\mathrm{Re}\big(jks_l(k)e^{j\omega_l k}e^{j(i\gamma_l)}n_i^*(k)\big)\big\} \tag{54}$$

and

$$\frac{\partial \ln(p(\mathbf{x}|\psi))}{\partial \theta_l} = \frac{1}{\sigma^2}\sum_{k=0}^{K-1}\sum_{i=-N+1}^{N}\left\{\mathrm{Re}\left[js_l(k)e^{j\omega_l k}e^{j(i\gamma_l)}\left(-\frac{2\pi di\sin\theta_l}{\lambda_l}\right)n_i^*(k)\right]\right\}. \tag{55}$$

Based on (49)–(52) (for near-field sources) or (53)–(55) (for far-field sources), we obtain $\frac{\partial \ln(p(\mathbf{x}|\psi))}{\partial \psi_l}$ for all L sources and then form the following column vector $\frac{\partial \ln(p(\mathbf{x}|\psi))}{\partial \psi}$ by using $\frac{\partial \ln(p(\mathbf{x}|\psi))}{\partial \psi_l}$:

$$\frac{\partial \ln(p(\mathbf{x}|\psi))}{\partial \psi} = \left[\frac{\partial \ln(p(\mathbf{x}|\psi))}{\partial \psi_1} \quad \cdots \quad \frac{\partial \ln(p(\mathbf{x}|\psi))}{\partial \psi_l} \quad \cdots \quad \frac{\partial \ln(p(\mathbf{x}|\psi))}{\partial \psi_L}\right]^T. \tag{56}$$

Based on (56), we obtain the Fisher information matrix $\mathbf{F}$ as follows:

$$\mathbf{F} = E\left[\frac{\partial \ln(p(\mathbf{x}|\psi))}{\partial \psi}\left(\frac{\partial \ln(p(\mathbf{x}|\psi))}{\partial \psi}\right)^T\right]. \tag{57}$$

Therefore, the CRLB on the variance of the estimated parameters can be obtained from the related diagonal elements of the inverse $\mathbf{F}^{-1}$ [20]. In this paper, the Fisher information matrix $\mathbf{F}$ is estimated by averaging the 500 computations of $\frac{\partial \ln(p(\mathbf{x}|\psi))}{\partial \psi}(\frac{\partial \ln(p(\mathbf{x}|\psi))}{\partial \psi})^T$ in the 500 independent Monte Carlo runs.

References

[1] H. Krim, M. Viberg, Two decades of array signal processing research: the parametric approach, IEEE Signal Process. Mag. 13 (4) (1996) 67–94.
[2] A.L. Swindelehurst, T. Kailath, Passive direction-of-arrival and range estimation for near-field sources, in: Fourth Annual ASSP Workshop on Spectrum Estimation and Modeling, Minneapolis, MN, 1988, pp. 123–128.
[3] Y.D. Huang, M. Barkat, Near-field multiple source localization by passive sensor array, IEEE Trans. Antennas Propag. 39 (7) (1991) 968–975.
[4] R. Schmidt, Multiple emitter location and signal parameter estimation, IEEE Trans. Antennas Propag. 34 (3) (1986) 276–280.
[5] R. Jeffers, K.L. Bell, H.L. Van Trees, Broadband passive range estimation using MUSIC, in: Proceedings of the IEEE International Conference on Acoustics, Speech, and Signal Processing, vol. 3, 2002, pp. 2921–2924.
[6] A.J. Weiss, B. Friedlander, Range and bearing estimation using polynomial rooting, IEEE J. Oceanic Eng. 18 (4) (1993) 130–137.
[7] D. Starer, A. Nehorai, Passive localization of near-field sources by path following, IEEE Trans. Signal Process. 42 (3) (1994) 677–680.
[8] E. Grosicki, K. Abed-Meraim, Y. Hua, A weighted linear prediction method for near-field source localization, IEEE Trans. Signal Process. 53 (10, 1) (2005) 3651–3660.
[9] K. Abed-Meraim, Y. Hua, A. Belouchrani, Second-order near-field source localization: algorithm and performance analysis, in: 30th Asilomar Conference on Signals, Systems & Computers, vol. 1, Pacific Grove, CA, 1997, pp. 723–727.
[10] E. Grosicki, K. Abed-Meraim, A weighted linear prediction method for near-field source localization, in: Proc. IEEE Int. Conf. Acoust. Speech Signal Process., vol. 3, 2002, pp. 2957–2960.
[11] N. Yuen, B. Friedlander, Performance analysis of higher order ESPRIT for localization of near-field sources, IEEE Trans. Signal Process. 46 (3) (1998) 709–719.
[12] R.N. Challa, S. Shamsunder, High-order subspace based algorithms for passive localization of near-field sources, in: 29th Asilomar Conference on Signals, Systems & Computers, vol. 2, Pacific Grove, CA, 1995, pp. 777–781.
[13] R. Roy, T. Kailath, ESPRIT-estimation of signal parameters via rotational invariance techniques, IEEE Trans. Acoust. Speech Signal Process. 37 (7) (1989) 984–995.
[14] J. Chen, X. Zhu, X. Zhang, A new algorithm for joint range–DOA–frequency estimation of near-field sources, EURASIP J. Appl. Signal Process. 2004 (3) (2004) 386–392.
[15] D.B. Ward, G.W. Elko, Mixed near field/far field beamforming: a new technique for speech acquisition in a reverberant environment, in: Proceedings of the IEEE ASSP Workshop on Applications of Signal Processing to Audio and Acoustics, New Paltz, NY, 1997, pp. 19–22.
[16] M. Agrawah, R. Abrahamsson, P. Ahgren, Optimum beamforming for a nearfield source in signal correlated interferences, Signal Process. 86 (5) (2006) 915–923.
[17] J.D. Lin, W.H. Fang, Y.Y. Wang, J.T. Chen, FSF MUSIC for joint DOA and frequency estimation and its performance analysis, IEEE Trans. Signal Process. 54 (12) (2006) 4529–4542.
[18] A.N. Lemma, A.J. van der Veen, E.F. Deprettere, Analysis of joint angle-frequency estimation using ESPRIT, IEEE Trans. Signal Process. 51 (5) (2003) 1264–1283.
[19] R.C. Johnson, Antenna Engineering Handbook, third ed., McGraw–Hill, pp. 9–12.
[20] S.M. Kay, Fundamentals of Statistical Signal Processing: Estimation Theory, Prentice Hall, Upper Saddle River, NJ, 1993.

Junli Liang was born in China, in 1978. He received the B.S. and M.S. degrees in computer science and technology in Xidian University, in 2001 and 2004, respectively. In 2007, he received his Ph.D. degree in signal and information processing in the Institute of Acoustics, Chinese Academy of Sciences. Currently, he is working in School of Computer Science and Engineering, Xi'an University of Technology. His research interests include adaptive filtering, array signal processing, pattern recognition, image processing, and intelligent signal processing.

Xianju Zeng was born in China, in 1978. He received his Ph.D. degree in management from School of Management, Xi'an Jiaotong University. Currently, he is working as a post-doctor in Department of management, City University of Hong Kong.

Bangjie Ji was born in China. He is the Dean of the National Key Laboratory for Underwater Information Process and Control. Currently, his research interests include underwater information processing and control.

Junying Zhang was born in China, in 1961. She received her Ph.D. degree in signal and information processing from Xidian University, Xi'an, China, in 1998. From 2001 to 2002, she was a visiting scholar at the Department of Electrical Engineering and Computer Science, the Catholic University of America, Washington, DC, USA. She is currently a Professor in the School of Computer Science and Engineering in Xidian University, Xi'an, China and presently is a short-time research professor in the Bradley Department of Electrical and Computer Engineering Institute in Virginia Tech University, Virginia, USA. Her research interests focus on intelligent information processing, machine learning and its application to disease related bioinformatics, image processing, radar automatic target recognition, and pattern recognition.

Feng Zhao was born in China, in 1974. He received his M.S. degree from the School of Computer Science and Engineering, Xidian University, Xi'an, China, in 2005. Currently, he is studying for his Ph.D. degree in signal and information processing in Xidian University. His research interests include intelligent signal and information processing.